

Kardar-Parisi-Zhang Interfaces with Inward Growth

Yohsuke T. Fukai^{1,2,*} and Kazumasa A. Takeuchi^{2,†}

¹*Department of Physics, the University of Tokyo*

²*Department of Physics, Tokyo Institute of Technology*

(Dated: October 2, 2018)

We study the $(1+1)$ -dimensional Kardar-Parisi-Zhang (KPZ) interfaces growing inward from ring-shaped initial conditions, experimentally and numerically, using growth of a turbulent state in liquid-crystal electroconvection and an off-lattice Eden model, respectively. To realize the ring initial condition experimentally, we introduce a holography-based technique that allows us to design the initial condition arbitrarily. Then, we find that fluctuation properties of ingrowing circular interfaces are distinct from those for the curved or circular KPZ subclass and, instead, are characterized by the flat subclass. More precisely, we find an asymptotic approach to the Tracy-Widom distribution for the Gaussian orthogonal ensemble and the Airy_1 spatial correlation, as long as time is much shorter than the characteristic time determined by the initial curvature. Near this characteristic time, deviation from the flat KPZ subclass is found, which can be explained in terms of the correlation length and the circumference. Our results indicate that the sign of the initial curvature has a crucial role in determining the universal distribution and correlation functions of the KPZ class.

The concept of universality class, which was originally introduced for equilibrium critical phenomena, is now extending its applicability to scale-invariant phenomena in out-of-equilibrium systems. It is then fundamental to ask whether one can characterize an out-of-equilibrium universality class as deeply as an equilibrium counterpart – such as the celebrated Ising class – and, if yes, whether it has something conceptually new in it. In this context, recent developments on the Kardar-Parisi-Zhang (KPZ) class [1–3], which describes fluctuations of growing interfaces as a notable example are particularly relevant. For the one-dimensional case, the KPZ class became analytically tractable by exact solutions to simple integrable models [3], which moreover showed intriguing *geometry dependence* as we shall state below.

When a d -dimensional interface separates two distinct regions in $(d+1)$ -dimensional space, and one region expands into the other in the presence of noise, the interface typically develops scale-invariant fluctuations, without fine tuning of the system parameters [2]. The KPZ class describes such an interface under generic conditions, without long-range interactions and conservation laws. It is represented by the KPZ equation [1], which reads, for interface height $h(x, t)$ at lateral position $x \in \mathbb{R}^d$ and time $t \in \mathbb{R}$,

$$\partial_t h(x, t) = \nu \nabla^2 h(x, t) + \frac{\lambda}{2} (\nabla h(x, t))^2 + \eta(x, t). \quad (1)$$

Here, η is a Gaussian noise satisfying $\langle \eta(x, t) \rangle = 0$ and $\langle \eta(x, t) \eta(x', t') \rangle = D \delta(x - x') \delta(t - t')$ and $\langle \dots \rangle$ denotes the ensemble average. Then the height $h(x, t)$ develops nontrivial fluctuations with amplitude $\sim t^\beta$ and correlation length $\sim t^{1/z}$. These exponents are universal – thus, the KPZ class is defined – as demonstrated by numerous growth models [2, 3] and a growing variety of experiments [4]: colony growth of living cells [5, 6], paper combustion [7], liquid-crystal electroconvection [8–10], particle deposition underlying coffee ring effect [11], chemical wave

fronts [12], etc. Theoretically, KPZ also arises in directed polymer problems [2, 3], fluctuating hydrodynamics [13], incompressible active matter [14], quantum entanglement under random unitary dynamics [15], and so on.

For the one-dimensional KPZ class, $\beta = 1/3$ and $z = 3/2$ [1, 2, 16], so that $h(x, t)$ can be expressed as follows:

$$h(x, t) \simeq v_\infty t + (\Gamma t)^{\frac{1}{3}} \chi(x', t) \quad (2)$$

where statistical variable $\chi(x', t)$ denotes rescaled height, x' is defined by $x' := x/\xi(t)$ with correlation length $\xi(t) := \frac{2}{A} (\Gamma t)^{2/3}$, and $v_\infty, A > 0$ and Γ are nonuniversal parameters. Recent studies on integrable models then unveiled exact statistical properties of $\chi(x', t)$ in $t \rightarrow \infty$ [3], in particular the distribution and spatial correlation functions, which were moreover shown to depend on the global geometry of interfaces. For example, (1) (globally) flat interfaces growing from a straight line, and (2) circular (or curved) interfaces starting from a point (or equivalent) were found to show different distribution functions: what arises is the largest-eigenvalue distribution of random matrices in the Gaussian orthogonal (unitary) ensemble [GOE (GUE) Tracy-Widom distribution [17]] in the flat (circular) case, respectively [18–23]. In other words, χ in Eq. (2) turned out to converge (in distribution) to different random variables, denoted by χ_1 (flat) and χ_2 (circular) [19]. Similarly, the spatial correlation was also shown to be different, namely the Airy_1 (flat) [20] and Airy_2 (circular) [24] correlation function.

This geometry dependence turned out to be relevant in real experiments also. Using liquid-crystal (LC) electroconvection, the authors of Refs.[8–10] studied growing clusters of turbulence, or more precisely, spatiotemporal chaos called the dynamic scattering mode 2 (DSM2), which invades another turbulent state, DSM1. The initial DSM2 cluster was nucleated by ultraviolet (UV) laser pulses focused on a point or a line, generating a circular or flat interface, respectively. These interfaces

were indeed shown to exhibit distinct properties, as described above for integrable models [9, 10]. Therefore, these properties are universal, yet geometry dependent; in other words, the KPZ class consists of a few different *universality subclasses*, characterized by the same exponents but different distribution and correlation properties. Importantly, the circular and flat subclasses may even have *qualitative* differences, such as algebraic (circular) vs superexponential (flat) decay of the spatial correlation function [25], persistence of time correlation in the circular case [10, 26, 27], etc. Theoretically, another subclass for stationary interfaces was also established [3].

However, in contrast to the detailed knowledge on each subclass, relevant parameters that determine the subclass still remain unclear. To shed light on this problem experimentally, here we developed a holography-based technique to generate an *arbitrary* initial condition of the DSM2 interface. Using this technique, we realized ring-shaped initial conditions and measured interfaces growing *inward* from the ring (Fig.1(b)). Although it is an experimentally natural geometry (e.g., coffee ring effect [11]), to our knowledge it has never been studied theoretically. One may guess that this would also lead to the circular subclass, because of the presence of the curvature, but it is not clear how the *sign* of the initial curvature intervenes. Our aim is to give a clear answer to this problem. Numerical simulations were also carried out to corroborate the experimental results.

The basic experimental setup for the LC electroconvection was similar to that used in [8–10]. We prepared a LC cell, which consisted of two glass plates with transparent electrodes, separated by spacers of $12\ \mu\text{m}$ thickness. Our LC sample, *N*-(4-Methoxybenzylidene)-4-butylaniline doped with 0.01 wt % of tetra-*n*-butylammonium bromide, was introduced to a $1.5\ \text{cm} \times 1.5\ \text{cm}$ area enclosed by the spacers. The electrodes were coated by *N,N*-dimethyl-*N*-octadecyl-3-aminopropyltrimethoxysilyl chloride to obtain the homeotropic alignment. The cutoff frequency separating the conductive and dielectric regimes [28] was 1.77(11) kHz. Then, DSM2 can be generated by shooting UV laser pulses to the cell, subjected beforehand to a relatively high voltage that drives the convection.

In order to realize arbitrary initial conditions, one needs to design the beam profile of the UV laser. To this end, we constructed an optical setup (Fig.1(a)) using a spatial light modulator (SLM, Hamamatsu Photonics, LCOS-SLM X10468-05), which allowed us to control the phase profile of the beam at the resolution of 792×600 pixels. We tuned the phase modulation by the iterative Fourier transform algorithm [29] until the Fourier-transformed image generated by the lens had an intensity profile close to the desired one [30]. Thereby, we were indeed able to design the initial DSM2 region arbitrarily (Fig.1(b)).

In this Letter, we focus on the case of ring-shaped ini-

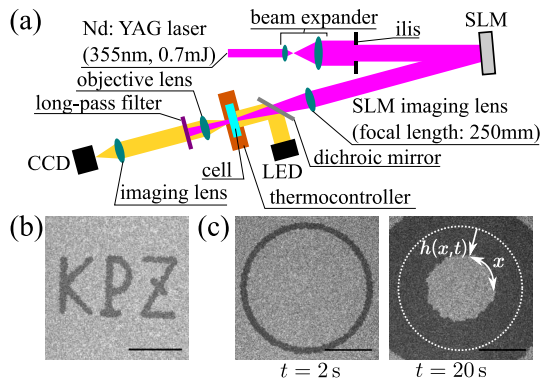


FIG. 1. (color online). (a) Schematic of the optical setup. Nd:YAG: neodymium-doped yttrium aluminum garnet, SLM: spatial light modulator, CCD: charge-coupled device camera, LED: light-emitting diode. The whole setup is placed in an isothermal chamber as in Ref.[10]. (b,c) Images of DSM2, growing from a “KPZ” initial condition (b) and a ring with $R_0 = 1342\ \mu\text{m}$ (c). For (c), the elapsed time after laser shooting is indicated below each image. The scale bar is 1 mm. The dotted line in the right figure indicates the estimated initial condition. See also Movies S1 and S2 [32].

tial conditions, as exemplified in Fig.1(c). During the experiment, the cell was attached to a temperature controller, whose temperature was maintained at $25\ ^\circ\text{C}$ with fluctuations of about $\pm 0.01\ ^\circ\text{C}$. The cell was illuminated by a light-emitting diode. For each realization, we started to apply 500 Hz 31 V AC voltage to the cell, shot UV laser pulses to generate a ring-shaped DSM2 region of radius R_0 , and recorded the ingrowing interface through the transmitted light by a charge-coupled device camera. We chose $R_0 = 1342\ \mu\text{m}$, $1241\ \mu\text{m}$ and $826\ \mu\text{m}$ and obtained more than 1500 samples for each case (see Table SI [31]). To define the height $h(x, t)$, we first determined the center of the ring, using the ensemble average of the images taken at the first frame used in the analysis. Then $h(x, t)$ was defined as the radial displacement from the initial ring estimated from the images at the first frame used in the analysis, and x is measured along the circumference, whose radius is equal to the mean radius of the interfaces at time t (Fig.1(c)). The overhangs were averaged out. We also obtained flat interfaces from the line initial condition.

To better understand the experimental results and check the universality, we also conducted simulations of ingrowing interfaces in an off-lattice Eden model [32], which is an isotropic model known to be in the KPZ class, but adapted here to the inward growth. The model consists of a cluster of round particles with unit diameter, which are added one by one stochastically in two-dimensional space. Starting from an initial condition composed of N circularly arranged particles, the model evolves following the rules described in [31]. We simulated ingrowing interfaces with $N = 8000, 16000, 32000, 100000$ and obtained

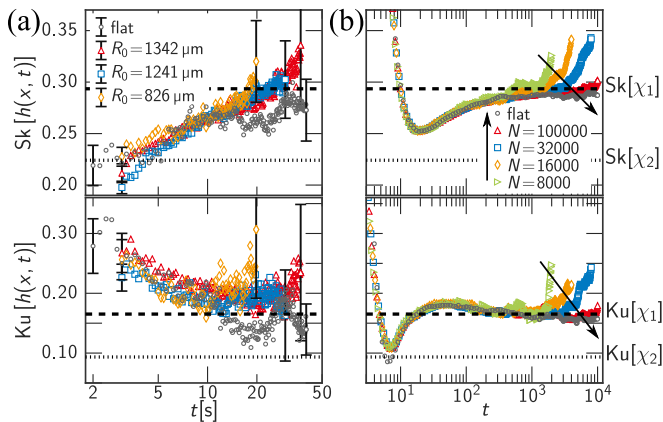


FIG. 2. (color online). Skewness and kurtosis. The values for χ_1 and χ_2 are shown by the dashed and dotted lines, respectively. (a) Experimental results. Statistical errors are indicated by the error bars, shown at the first and last data points. (b) Numerical results. The arrows indicate decreasing initial curvature.

2400, 3200, 3200, 1600 realizations, respectively. The initial radius R_0 is given by $R_0 = N/2\pi$. We also obtained 3200 flat interfaces using the line initial condition of length 25000.

First, we measured the n th-order cumulants of $h(x, t)$ [33], denoted by $\langle h^n \rangle_c$, and evaluated the skewness $\text{Sk}[h] := \langle h^3 \rangle_c / \langle h^2 \rangle_c^{3/2}$ and the kurtosis $\text{Ku}[h] := \langle h^4 \rangle_c / \langle h^2 \rangle_c^2$. Figure 2(a) and (b) show the results for the LC experiment and the Eden model, respectively. In both cases, after initial transient, the values for the flat interfaces agree with those for χ_1 , i.e., the GOE Tracy-Widom distribution, as expected. Curiously, for the ingrowing cases, too, no sign of the circular subclass was found, but the initial transient data agreed with those of the flat interfaces. For the Eden model (Fig. 2(b)), the skewness and kurtosis then reached and stayed for a while at the χ_1 values, until they eventually deviated in the direction opposite to the χ_2 values, at some characteristic times dependent on the initial curvature.

In order to investigate the cumulants of the rescaled height $\chi(x', t)$ and its spatial correlation, we estimated the nonuniversal parameters v_∞ and Γ . Experimentally, we determined the parameters for each set of experiments, because of the possible change of the parameter values [10]. For the flat interfaces, we evaluated v_∞ from the mean growth speed by using $\langle \partial_t h \rangle \simeq v_\infty + \text{const.} \times t^{-2/3}$, and Γ from the variance by fitting $\langle h(x, t)^2 \rangle_c t^{-2/3} \simeq \Gamma^{2/3} \langle \chi_1^2 \rangle_c + \text{const.} \times t^{-2/3}$ [10] (Fig. S1 [31]). For the ingrowing interfaces, on the basis of the observation that the early-time behavior of the skewness and kurtosis overlaps with that of the flat interfaces (Fig.2), we assumed that time series of individual cumulants, when properly rescaled, also overlap with the flat data, and thereby determined v_∞ and Γ (see [31]

for details). The estimated parameter values are summarized in Table SI [31]. For the Eden model, since the nonuniversal parameters are expected not to depend on the geometry [10, 19], we used the estimates from extensive simulations in Ref.[34], while using the values in Ref.[32] did not change the conclusion drawn below. For both cases, the parameter A is given by $A = \sqrt{2\Gamma}/v_\infty$ that holds for isotropic systems [10].

Using these estimates, we obtained the rescaled height

$$q(x', t) := (\Gamma t)^{-1/3} (h(x, t) - v_\infty t) \simeq \chi(x', t) \quad (3)$$

and evaluated the cumulants $\langle q^n \rangle_c \simeq \langle \chi(x', t)^n \rangle_c$ up to $n = 4$. As for the mean $\langle q \rangle$, since it is sensitive to the estimation of R_0 and has a large finite-time effect [9, 10, 32], we used instead the mean value of the rescaled velocity

$$\langle p(x', t) \rangle := \left\langle \frac{3t^{2/3}}{\Gamma^{1/3}} (\partial_t h(x, t) - v_\infty) \right\rangle \simeq \langle \chi(x', t) \rangle \quad (4)$$

to compare with $\langle \chi(x', t) \rangle$.

The experimental and numerical data for the mean rescaled velocity $\langle p \rangle$ and the variance $\langle q^2 \rangle_c$ are plotted in Figs. 3(a)-3(d). As expected, the values for the flat interfaces converge to $\langle \chi_1 \rangle$ and $\langle \chi_1^2 \rangle_c$, respectively. The ingrowing data were found to approach the corresponding cumulants of χ_1 in a way similar to the flat case, but eventually deviate at some characteristic time, which becomes larger for larger R_0 (i.e. smaller initial curvature). In all cases, no sign of approach to $\langle \chi_2 \rangle$ and $\langle \chi_2^2 \rangle_c$ was found, similarly to the results of the skewness and kurtosis (Fig.2). Consistent behaviors were found in the third- and fourth-order cumulants (Fig. S2 [31]), despite relatively large statistical error. We also measured the two-point spatial correlation function $C_s(\zeta, t) := \text{Cov}[q(x' + \zeta, t), q(x', t)]$ for the ingrowing interfaces [Figs. 2(e) and 2(f)]. While $\langle p \rangle$ and $\langle q^2 \rangle_c$ are approaching $\langle \chi_1 \rangle$ and $\langle \chi_1^2 \rangle_c$, respectively, $C_s(\zeta, t)$ approaches the Airy_1 correlation [see the circular and square bullets in Figs. 3(e) and 3(f) and compare with the black solid line], which is the hallmark of the flat subclass. After $\langle p \rangle$ and $\langle q^2 \rangle_c$ deviate from the values of the flat interfaces, $C_s(\zeta, t)$ also deviates from the Airy_1 correlation [the triangle bullets in Figs. 3(e) and 3(f)]. In any case, $C_s(\zeta, t)$ was clearly different from the Airy_2 correlation (black dashed line) for the circular subclass.

The results so far indicate, both experimentally and numerically, that it is the *flat* subclass that characterizes the ingrowing interfaces, until the deviation eventually occurs at some characteristic time. Then what controls this deviation regime? Let us remark here that ingrowing interfaces eventually collapse near the center of the ring, when $\langle h \rangle \simeq v_\infty t$ reaches R_0 . This led us to rescale time as $\tau := t/t_c = v_\infty t/R_0$ with $t_c := R_0/v_\infty$ being the (approximate) collapse time. Figures 4(a) and 4(c) show the numerical data of the mean rescaled velocity $\langle p \rangle$ and

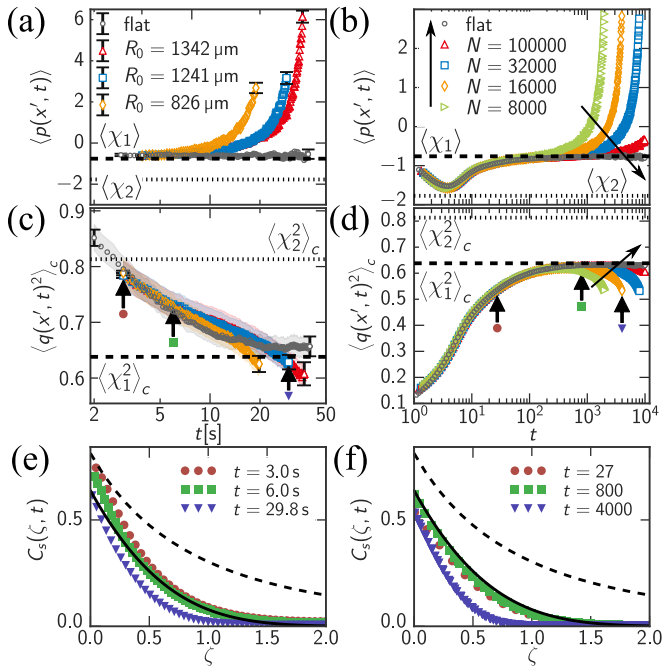


FIG. 3. (color online). Rescaled fluctuation properties. (a-d) Mean rescaled velocity $\langle p(x, t) \rangle$ (a, b) and the variance $\langle q(x, t)^2 \rangle_c$ (c, d) for the LC experiment (a, c) and the Eden model (b, d). The statistical errors are shown by the error bars at the first and last data points in (a, c). The confidence interval associated with the estimation of the nonuniversal parameters is indicated by the shaded area in (c), while it is smaller than the marker size in (a). The arrows in (b, d) indicate decreasing initial curvature. The horizontal lines indicate the mean or variance of χ_1 (dashed lines) and χ_2 (dotted lines). (e, f) The spatial correlation function $C_s(\zeta, t)$ for the LC experiment with $R_0 = 1241 \mu\text{m}$ (e), and for the Eden model with $N = 16000$ (f). The solid and dashed lines indicate the Airy_1 and Airy_2 correlation function, respectively.

variance $\langle q^2 \rangle_c$, plotted against this rescaled time, and indeed the data collapsed well in the deviation regime. It is reasonable that the deviation occurs near $t \approx t_c$, because the correlation length $\xi(t) \sim t^{2/3}$ then reaches the effective system size, or the circumference, $L(t) = 2\pi(R_0 - \langle h \rangle) \simeq 2\pi(R_0 - v_\infty t)$. In contrast, in the short-time regime $t \ll t_c$, we expect that the asymptotic curves of the cumulants $\langle q^n \rangle_c$, obtained in the limit $R_0, t \rightarrow \infty$ with fixed $\tau \ll 1$, converge to $\langle \chi_1^n \rangle_c$ as $\tau \rightarrow 0$, which corresponds to the flat limit ($R_0 \rightarrow \infty$).

We also made the same rescaling with the experimental data and found that $\langle p \rangle$ against τ overlaps on the curve of the Eden model within the error [Fig. 4(b)], suggesting universality of this scaling function. Concerning $\langle q^2 \rangle_c$, the experimental data do not overlap with the Eden curve [Fig. 4(d)], but the deviation is smaller for larger R_0 ; therefore the two curves possibly overlap in $R_0 \rightarrow \infty$, though the experimentally reachable value of R_0 is far too small to make a direct verification.

In summary, we developed an experimental technique

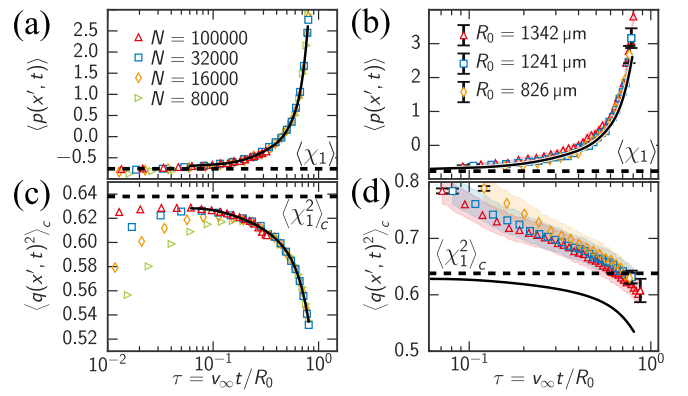


FIG. 4. (color online). The mean rescaled velocity $\langle p(x, t) \rangle$ (a), (b) and the variance $\langle q(x, t)^2 \rangle_c$ (c), (d) against rescaled time $\tau = v_\infty t / R_0$ for the Eden numerics (a, c) and for the LC experiment (b, d). For the experimental data, the errors are indicated in the same way as Fig. 3(a, c). The black solid lines are the spline-curve fit of the Eden data with $t \geq 10^3$. The dashed lines show the mean or variance of χ_1 .

that allowed us to design the initial region of the DSM2 turbulence arbitrarily. This opens a way to study KPZ interfaces from general initial conditions, experimentally, providing a basis for investigating the intriguing geometry dependence of the KPZ class.

Then we studied interfaces growing inward from a ring, both experimentally and numerically, using for the latter the off-lattice Eden model. In the short-time regime ($t \ll t_c = R_0 / v_\infty$), our cumulant data [Figs. 2 and 3(a)-3(d)] agreed with those for the flat interfaces, indicating that they are asymptotic to those of the GOE Tracy-Widom distribution. In this regime the spatial correlation function was also approaching the Airy_1 correlation, which is another hallmark of the flat subclass. The circular subclass scenario was clearly ruled out. Therefore, not only the presence of the curvature but its sign have a crucial effect on the determination of the universality subclass. By contrast, in the long-time regime close to the collapse time $\approx t_c = R_0 / v_\infty$, the fluctuations were no longer controlled by the flat KPZ subclass. The cumulants in this regime were found to be parametrized by dimensionless time $\tau = t / t_c$ (Fig. 4), implying the existence of scaling functions for this regime. This long-time behavior is argued to occur as the correlation length $\xi(t)$ becomes comparable to the effective system size $L(t)$.

Our results may arouse a few interesting discussions. First, why does the sign of the initial curvature matter? Although firm theoretical understanding needs to be made, our arguments based on the effective system size may give a tentative answer: while for the usual outgrowing circular interfaces the correlation length $\xi(t) \sim t^{2/3}$ never attains the effective system size $L(t) \sim t$, in our ingrowing case, this does happen, as $L(t)$ now decreases in time. Earlier numerical work [35] indeed showed that the system size expansion is crucial for the circular subclass.

Second, we note that ingrowing interfaces arise naturally in some systems, in particular in the coffee-ring experiment [11], where particles in a droplet accumulate onto the droplet edge. This experiment needs to be revisited, because the data were compared with the GUE Tracy-Widom distribution. There is also a model on the quantum entanglement entropy whose connection to KPZ was shown [15]; in this model, the size of the growth region decreases in time, similarly to the ingrowing geometry we study here. From broader perspectives, we remark that the split to universality subclasses occurs not only in KPZ, but also in another class of nonlinear growth problems [36]. Analogous geometry dependence was also suggested for absorbing-state phase transitions [37]. We hope our work will trigger further experimental and theoretical studies to elucidate this geometry dependence, which may be a new aspect of such out-of-equilibrium scaling laws.

We acknowledge discussions on the experimental and numerical methods with M. Sano, on theoretical aspects with T. Sasamoto, H. Spohn, P. Le Doussal, H. Chaté, on interpretations of the results with R. A. L. Almeida. We thank H. Spohn for having drawn our attention to Ref.[15], suggesting possible connection to our work. We also thank F. Bornemann for the theoretical curve of the Airy_1 and Airy_2 correlation functions [38] and M. Kuroda for technical support. Japan Society for the Promotion of Science (Grants No. JP25103004, No. JP16H04033, No. JP16K13846) and the National Science Foundation under Grant No. NSF PHY11-25915.

* ysk@yukai.net

† kat@kaztake.org

- [1] M. Kardar, G. Parisi, and Y.-C. Zhang, Phys. Rev. Lett. **56**, 889 (1986).
- [2] A.-L. Barabási and H. E. Stanley, *Fractal Concepts in Surface Growth* (Cambridge University Press, New York, NY, USA, 1995).
- [3] For recent reviews on theoretical studies, see T. Kriecherbauer and J. Krug, J. Phys. A: Math. Theor. **43**, 403001 (2010); I. Corwin, Random Matrices Theory Appl. **01**, 1130001 (2012); J. Quastel and H. Spohn, J. Stat. Phys. **160**, 965 (2015); T. Halpin-Healy and K. A. Takeuchi, J. Stat. Phys. **160**, 794 (2015); T. Sasamoto, Prog. Theor. Exp. Phys. **2016**, 022A01 (2016) etc.
- [4] See K. A. Takeuchi, J. Stat. Mech. Theor. Exp. **2014**, P01006 (2014) for a review on experiments.
- [5] J.-i. Wakita, H. Itoh, T. Matsuyama, and M. Matsushita, J. Phys. Soc. Jpn. **66**, 67 (1997).
- [6] M. A. C. Huergo, M. A. Pasquale, A. E. Bolzán, A. J. Arvia, and P. H. González, Phys. Rev. E **82**, 031903 (2010); M. A. C. Huergo, M. A. Pasquale, P. H. González, A. E. Bolzán, and A. J. Arvia, Phys. Rev. E **84**, 021917 (2011); Phys. Rev. E **85**, 011918 (2012).
- [7] J. Maunukela, M. Myllys, O.-P. Kähkönen, J. Timonen, N. Provatas, M. J. Alava, and T. Ala-Nissila, Phys. Rev. Lett. **79**, 1515 (1997); M. Myllys, J. Maunukela, M. Alava, T. Ala-Nissila, J. Merikoski, and J. Timonen, Phys. Rev. E **64**, 036101 (2001).
- [8] K. A. Takeuchi and M. Sano, Phys. Rev. Lett. **104**, 230601 (2010).
- [9] K. A. Takeuchi, M. Sano, T. Sasamoto, and H. Spohn, Sci. Rep. **1**, 34 (2011).
- [10] K. A. Takeuchi and M. Sano, J. Stat. Phys. **147**, 853 (2012).
- [11] P. J. Yunker, M. A. Lohr, T. Still, A. Borodin, D. J. Durian, and A. G. Yodh, Phys. Rev. Lett. **110**, 035501 (2013).
- [12] S. Atis, A. K. Dubey, D. Salin, L. Talon, P. Le Doussal, and K. J. Wiese, Phys. Rev. Lett. **114**, 234502 (2015).
- [13] H. Spohn, Lect. Notes Phys. **921**, 107 (2016).
- [14] L. Chen, C. F. Lee, and J. Toner, Nat. Commun. **7**, 12215 (2016).
- [15] A. Nahum, J. Ruhman, S. Vijay, and J. Haah, Physical Review X **7**, 031016 (2017).
- [16] D. Forster, D. R. Nelson, and M. J. Stephen, Phys. Rev. A **16**, 732 (1977).
- [17] G. W. Anderson, A. Guionnet, and O. Zeitouni, *An Introduction to Random Matrices* (Cambridge University Press, 2010).
- [18] K. Johansson, Comm. Math. Phys. **209**, 437 (2000).
- [19] M. Prähofer and H. Spohn, Phys. Rev. Lett. **84**, 4882 (2000).
- [20] T. Sasamoto, J. Phys. A: Math. Gen. **38**, L549 (2005).
- [21] P. L. Ferrari and H. Spohn, J. Phys. A: Math. Gen. **38**, L557 (2005).
- [22] T. Sasamoto and H. Spohn, Phys. Rev. Lett. **104**, 230602 (2010); G. Amir, I. Corwin, and J. Quastel, Commun. Pure Appl. Math. **64**, 466 (2011); P. Calabrese, P. L. Doussal, and A. Rosso, EPL **90**, 20002 (2010); V. Dotseenko, EPL **90**, 20003 (2010).
- [23] P. Calabrese and P. Le Doussal, Phys. Rev. Lett. **106**, 250603 (2011).
- [24] M. Prähofer and H. Spohn, J. Stat. Phys. **108**, 1071 (2002).
- [25] F. Bornemann, P. L. Ferrari, and M. Prähofer, J. Stat. Phys. **133**, 405 (2008).
- [26] K. A. Takeuchi and T. Akimoto, J. Stat. Phys. **164**, 1167 (2016).
- [27] J. De Nardis, P. Le Doussal, and K. A. Takeuchi, Phys. Rev. Lett. **118**, 125701 (2017).
- [28] P. G. de Gennes and J. Prost, *The Physics of Liquid Crystals* (Oxford Science Publications, 1995).
- [29] F. Wyrowski and O. Bryngdahl, J. Opt. Soc. Am. A **5**, 1058 (1988).
- [30] We noticed that a tiny fraction of light was reflected by SLM without phase modulation, and caused uncontrolled DSM2 nucleation. To avoid this problem, we shifted the effective focal distance of the imaging lens, by superimposing a phase difference equivalent to a convex lens at SLM.
- [31] See Supplemental Material at <http://link.aps.org/supplemental/10.1103/PhysRevLett.119.030602> for the detailed evolution rules of the Eden model, nonuniversal parameter estimation for ingrowing interfaces, Table SI, Figs. S1 and S2, and Movies S1 and S2.
- [32] K. A. Takeuchi, J. Stat. Mech. Theor. Exp. **2012**, P05007 (2012).
- [33] When we calculated the cumulants from the experimental

data, we evaluated the cumulants of the fluctuations at each x and averaged them, in order to reduce the effect of heterogeneity of the cell and the initial condition.

- [34] S. G. Alves, T. J. Oliveira, and S. C. Ferreira, *J. Stat. Mech. Theor. Exp.* **2013**, P05007 (2013).
- [35] I. S. S. Carrasco, K. A. Takeuchi, S. C. Ferreira, and T. J. Oliveira, *New J. Phys.* **16**, 123057 (2014).
- [36] I. S. S. Carrasco and T. J. Oliveira, *Phys. Rev. E* **94**, 050801 (2016).
- [37] M. O. Lavrentovich, K. S. Korolev, and D. R. Nelson, *Phys. Rev. E* **87**, 012103 (2013).
- [38] F. Bornemann, *Math. Comp.* **79**, 871 (2010).